Heavy-Quark Diffusion and Hadronization in Quark-Gluon Plasma

Min He,[1] Rainer J. Fries,[1,2] and Ralf Rapp[1]

[1] *Cyclotron Institute and Department of Physics and Astronomy, Texas A&M University, College Station, TX 77843, USA*

[2] *RIKEN/BNL Research Center, Brookhaven National Laboratory, Upton, NY 11973, USA*

(Dated: June 30, 2011)

We calculate diffusion and hadronization of heavy quarks in high-energy heavy-ion collisions implementing the notion of a strongly coupled quark-gluon plasma in both micro- and macroscopic components. The diffusion process is simulated using relativistic Fokker-Planck dynamics for elastic scattering in a hydrodynamic background. The heavy-quark transport coefficients in the medium are obtained from non-perturbative T-matrix interactions which build up resonant correlations close to the transition temperature. The latter also form the basis for hadronization of heavy quarks into heavy-flavor mesons via recombination with light quarks from the medium. The pertinent resonance recombination satisfies energy conservation and provides an equilibrium mapping between quark and meson distributions. The recombination probability is derived from the resonant heavy-quark scattering rate. Consequently, recombination dominates at low transverse momentum (p_T) and yields to fragmentation at high p_T. Our approach thus emphasizes the role of resonance correlations in the diffusion and hadronization processes. We calculate the nuclear modification factor and elliptic flow of D- and B-mesons for Au-Au collisions at the Relativistic Heavy Ion Collider, and compare their decay-electron spectra to available data. We also find that a realistic description of the medium flow is essential for a quantitative interpretation of the data.

PACS numbers: 25.75.Dw, 12.38.Mh, 25.75.Nq
Keywords: Heavy Quark Diffusion, Quark Gluon Plasma, Quark Recombination

I. INTRODUCTION

Experiments at the Relativistic Heavy Ion Collider (RHIC) and the Large Hadron Collider (LHC) have been searching for the deconfined phase of nuclear matter and have begun to probe its properties [1, 2]. There are strong indications that this new form of matter behaves like a nearly perfect fluid with high opacity and low viscosity, referred to as strongly coupled Quark-Gluon Plasma (sQGP) [3, 4]. One of the major experimental findings is a large azimuthal anisotropy, v_2, in transverse momentum (p_T) spectra of hadrons in non-central collisions [5]. To account for this observation, hydrodynamic simulations require an early initialization time, implying a rapid thermalization of the bulk medium [6–8]. However, the microscopic origin of the rapid thermalization remains a matter of debate.

In contrast to light partons making up the bulk of the medium, heavy quarks (charm and bottom), produced in primordial hard collisions and acting as impurities in the QGP, are not expected to fully equilibrate with the surrounding medium. Due to their large masses (m_Q) a memory of their interaction history may be preserved, thus providing a more direct probe of the medium properties than bulk observables [9–12]. The thermal relaxation time of heavy quarks has been argued to be larger than that of light quarks by a factor of $m_Q/T \approx 5-20$ [11, 12] (T: typical temperature of the QGP). As they diffuse through the medium, heavy quarks interact with the light partons and their spectrum becomes quenched [10, 11]. Moreover, as they couple to the collective flow of the medium in non-central heavy-ion collisions, heavy quarks may develop substantial momentum anisotropies. These two effects are translated into equivalent behavior of heavy-flavor (HF) meson (D and B) spectra and v_2, and further into the spectrum and v_2 of their decay electrons. The latter have been measured in Au+Au collisions at RHIC [13–15], exhibiting appreciable modifications over their baseline spectra from $p+p$ and d+Au collisions.

Model calculations based on radiative energy loss in perturbative QCD (pQCD), which could account for the observed jet-quenching in the light sector [16], predicted a much smaller quenching for heavy quarks and associated single-electron spectra [17]. The large HQ mass suppresses small-angle gluon radiation ("dead cone" effect [18]) and reduces the gluon formation time [19], hence mitigating radiative energy loss significantly. However, elastic collisions of heavy quarks with light partons [9–11, 20, 21] have been argued to dominate over radiative scattering at low momentum, resulting in notable quenching of the HQ spectrum.

However, jet quenching only captures part of the physics potential of the HQ probe. Its diffusion properties, which reach all the way to zero momentum, include energy-gain processes which are, e.g., instrumental for the coupling to the collective flow of the medium. Several studies of HQ diffusion have been conducted in recent years using Fokker-Planck [10, 11, 21–27] and Boltzmann transport [28–30] approaches, mostly implementing elastic collisions as the microscopic dynamics. They differ not only in their treatment of the background medium, but also in the evaluation of (a) the transport coefficients emerging from the interactions between the heavy quarks and the medium, and (b) hadronization of

heavy quarks into HF mesons. Concerning item (a), most studies employ variants of the pQCD interaction [31], while a novel approach with heavy-light resonant interactions was introduced in Refs. [10, 22]. The latter was found to be a factor of 3-4 more efficient in HQ thermalization than pQCD, and was subsequently corroborated by microscopic T-matrix calculations using input potentials from lattice QCD (lQCD) [23, 32, 33]. Concerning HQ hadronization, several studies focused on independent fragmentation [25–27, 30], which is not reliable in the low and intermediate-p_T regimes. Here, light partons surrounding the heavy quark have a high phase-space density which renders coalescence a more plausible hadronization mechanism [35–38]. In Refs. [22, 23], heavy-light quark recombination has been incorporated utilizing an instantaneous coalescence model [39] which could still be problematic at low p_T due to lack of energy conservation. A reliable treatment of the low-p_T regime is important since the total number of heavy quarks is expected to be conserved through the hadronization transition. If the D- or B-meson spectra are distorted at low p_T, the spectra at higher p_T are necessarily affected thus modifying the R_{AA} (and v_2) of D and B-mesons and their decay electrons.

The purpose of the present work is to establish a realistic and quantitative framework for HQ probes within (a) a strongly coupled QGP background medium (modeled by hydrodynamics), (b) a non-perturbative scenario of elastic diffusion in the QGP simulated by Fokker-Planck-Langevin dynamics, and (c) a hadronization scheme at the phase transition based on the same interaction as in (b), combining recombination and fragmentation consistent with the limiting cases of kinetic equilibrium and vacuum hadronization. Unlike previous studies utilizing weak-coupling diffusion [11, 24, 26, 27, 30] we try to implement the HQ probe consistently within a framework of strong coupling between heavy and light quarks, both in the QGP and during hadronization. Our comprehensive framework is hence conceptually compatible with the notion of a strongly interacting QGP.

The strategy in this work is as follows. For the HQ transport coefficient we employ a non-perturbative T-matrix calculation of heavy-light quark interactions [32, 33]. This calculation supports Feshbach resonances in the QGP in the color-singlet and anti-triplet channels, surviving as rather broad states up to $\sim 1.5\ T_c$. They are responsible for the enhancement of the transport coefficient compared to pQCD scattering. With these coefficients we perform Langevin simulations of HQ diffusion through an expanding medium which is described by ideal 2+1-dimensional hydrodynamics (using the AZHYDRO code [40] at RHIC energies). At the phase transition, heavy quarks are hadronized through coalescence with light quarks of the medium using the Resonance Recombination Model (RRM) [41] implemented on a hypersurface given by the hydrodynamic simulation. The coalescence probability is evaluated using the resonant scattering rate of the heavy quark with light (anti) quarks, supplemented by independent fragmentation. The RRM formalism is consistent with the heavy-light Feshbach resonance formation found in the T-matrix used for the transport coefficient. This stipulates the role played by the resonance correlations in our work. With an artificially large transport coefficient, we check the equilibrium limit of the HQ distribution emanating from the combined hydro+Langevin simulation and the ensuing degree of equilibration of the HF mesons upon resonance recombination. The full space-momentum correlations generated by the hydro-Langevin simulation enter into resonance recombination. This enables a quantitative assessment of the radial medium flow on HF meson spectra at low p_T as imprinted on the final R_{AA} measurement.

Our article is organized as follows. In Sec. II we introduce the ingredients for the hydro-Langevin simulation of HQ diffusion in the medium, i.e., the transport coefficient, the initial distribution in coordinate and momentum space, and the background medium described by an ideal hydrodynamic model. Numerical results for the HQ R_{AA} and v_2 are discussed in the equilibrium limit as well as for realistic coefficients. Sec. III is devoted to HQ hadronization. We implement the RRM formalism on arbitrary hadronization hypersurfaces, elaborate the equilibrium mapping in resonance recombination, and determine the partition of coalescence and fragmentation. In Sec. IV we examine consequences of modifying the medium flow for the predicted HF meson spectra, triggered by indications that the partonic flow of the hydrodynamic evolution is too soft. In Sec. V we make contact with current experiments in terms of the nuclear modification factor and the elliptic flow of electrons from HF decays. In Sec. VI we summarize and conclude.

II. LANGEVIN SIMULATION OF HEAVY QUARK DIFFUSION

A. Relativistic Langevin Kinetics

The thermal momentum of a heavy quark at temperatures characteristic for heavy-ion collisions at RHIC amounts to $p_{th} \sim \sqrt{m_Q T}$, which is parametrically larger than the typical momentum transfer, $q \sim T$, in a single elastic collision with a light parton from the bulk medium. Therefore many collisions are needed to change the HQ momentum considerably [10, 11]. This forms the basis for approximating the HQ motion in the QGP by a succession of uncorrelated momentum kicks and leads to a Fokker-Planck approach realized stochastically by the Langevin equations [9, 12, 42, 43]

$$d\mathbf{x} = \frac{\mathbf{p}}{E} dt, \tag{1}$$

$$d\mathbf{p} = -\Gamma(p)\ \mathbf{p}\ dt + \sqrt{2D(\mathbf{p}+d\mathbf{p})\, dt}\ \rho\ , \tag{2}$$

where $\mathbf{x}$ and $\mathbf{p}$ are the position and momentum vector of the heavy quark, and $E(p) = (m_Q^2 + \mathbf{p}^2)^{1/2}$ is its energy. In the following we employ the post-point discretization

scheme in which the equilibrium condition (the relativistic fluctuation-dissipation theorem) takes the simple form

$$D(p) = \Gamma(p)\ E(p)\ T \tag{3}$$

with $\Gamma(p)$ being the drag coefficient and $D(p)$ the (diagonal) diffusion coefficient. The standard Gaussian noise variable, ρ, is distributed according to

$$w(\rho) = \frac{1}{(2\pi)^{3/2}} e^{-\rho^2/2}\,. \tag{4}$$

Neither the original Fokker-Planck equation [12, 42] nor the Langevin equation is Lorentz covariant. We choose the momentum and position updates for our HQ test particles to be at equidistant time steps $d\tau$ in the lab frame. For a flowing medium, as in our context, the momentum updates are rather to be done in the fluid rest frame. The updated 4-momentum is boosted back to the lab frame with the fluid four-velocity $u^\mu(x) = \gamma(v)(1, \mathbf{v}(x))$. The aforementioned equilibrium condition must be satisfied in order for the long-time limit of the test particle distribution to converge to the equilibrium (Boltzmann-Jüttner) distribution as defined by the underlying background medium. Further details of our algorithm will be detailed in a forthcoming article [44].

B. Thermal Relaxation Rate of Heavy Quarks

The transport coefficient most commonly calculated from an underlying microscopic interaction of the heavy quark with the bulk medium is the thermal relaxation rate $A(p;T)$. It is related to the drag coefficient, $\Gamma(p;T)$, in the post-point Langevin scheme, Eq. (2), through

$$\Gamma(p;T) = A(p;T) + \frac{1}{E(p)} \frac{\partial D(p;T)}{\partial E(p)}\ . \tag{5}$$

Utilizing the equilibrium condition (3) one can argue that $\Gamma(p) = A(p) + \mathcal{O}(T/m_Q)$ and neglect terms to higher order in the inverse HQ mass (relative to the medium temperature).

We employ HQ relaxation rates from Refs. [32], where in-medium T-matrices have been calculated for both heavy-light and quarkonium channels. The input potentials were constructed using a field-theoretic ansatz for a confining and a color-Coulomb interaction with parameters fitted to color-average free energies computed in finite-temperature lattice QCD (lQCD) [45]. This approach treats heavy quarkonia and heavy-light interactions in the QGP on an equal footing, and in both bound-state and scattering regimes. One thus obtains mutual constraints by analyzing, e.g., Euclidean correlation functions and HQ susceptibilities which turn out to agree fairly well with thermal lQCD "data" [33]. For heavy-light quark scattering, the (non-perturbative) resummation in the T-matrix generates resonances close to the 2-particle threshold (commonly referred to as "Feshbach resonances") in the attractive color-singlet (meson) and color-anti-triplet (diquark) channels up to temperatures of about $1.5\,T_c$, see Fig. 1 for charm quarks (similar results are obtained in the bottom sector). The increasing strength of the T-matrices in the color-singlet and anti-triplet channels when approaching T_c from above is indicative for "pre-hadronic" correlations leading to hadronization. But even at high temperatures a substantial enhancement of the T-matrix over elastic pQCD amplitudes persists, in particular close to threshold. The rather large resonance widths are mostly generated through the self-energies of the light- and heavy-quark propagators in the T-matrix (evaluated self-consistently in the HQ sector).

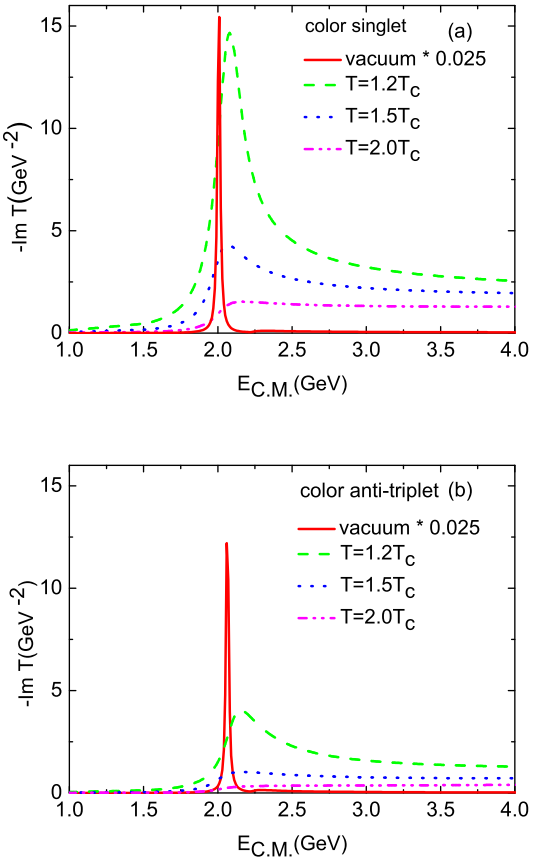

FIG. 1: (Color online) Imaginary part of the in-medium on-shell T-Matrix for charm-light quark scattering as a function of center-of-mass energy in the color-singlet (upper panel) and anti-triplet (lower panel) channels, taken from the lattice-QCD based potential approach of Ref. [32]. The vacuum T-matrices have been downscaled by a factor of 0.025.

The T-matrices have been used to calculate thermal relaxation rates of heavy quarks [32, 33]. Resonant rescattering accelerates kinetic equilibration by up to a factor of ∼3-5 relative to leading order (LO) pQCD calculations [9], cf. upper panel of Fig. 2. With increasing HQ 3-momentum the thermal phase space of comoving partons (suitable for forming a Feshbach resonance) de-

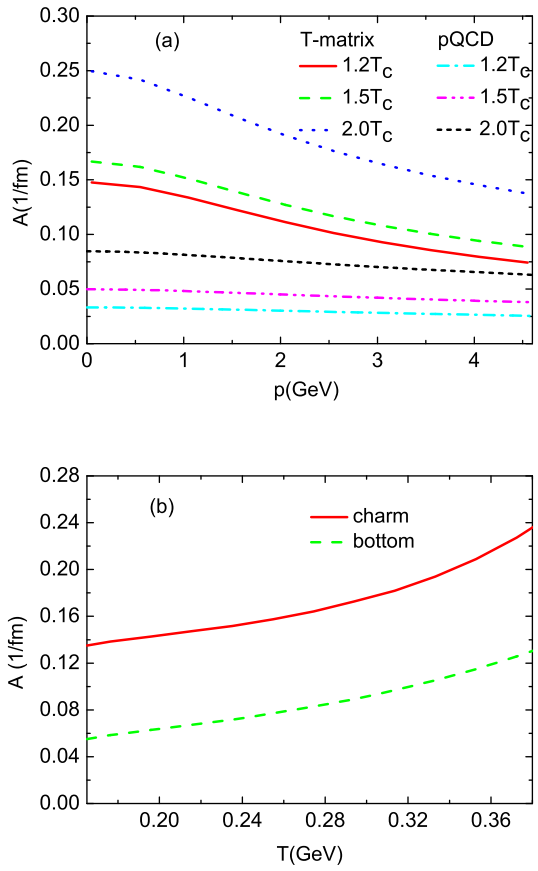

FIG. 2: (Color online) (a) Charm-quark relaxation rate as a function of three-momentum using (i) heavy-light quark T-matrices (with lQCD internal energy [45] as potential) plus pQCD gluon scattering with $\alpha_s = 0.4$ (upper 3 curves), and (ii) pQCD scattering off anti-/quarks and gluons with $\alpha_s = 0.4$ (lower 3 curves). (b) Temperature dependence of the charm/bottom quark thermal relaxation rate (at vanishing momentum) used in our simulations. The results are taken from Ref. [32].

creases and the relaxation rate approaches the pQCD results. For high energies and in Born approximation the T-matrix results recover the LO pQCD scattering amplitudes [32]. The temperature dependence of the charm and bottom relaxation rates (at vanishing 3-momentum) used in our simulations is displayed in the lower panel of Fig. 2. They have been extrapolated linearly from the transition temperature in the lQCD calculations of the free energies [45], T_c=196 MeV, to T_c=165 MeV implicit in the equation of state as used in AZHYDRO.

C. The hydrodynamic background QGP medium

Hydrodynamic simulations are widely applied to model the bulk evolution of the matter created in heavy-ion collisions at RHIC [6–8], providing a good description of hadron spectra and their elliptic flow. Here we use a hydrodynamic simulation of the fireball to provide the background medium for HQ diffusion. It supplies the information on the space-time evolution of energy and entropy density, as well as temperature and fluid velocity which are needed to calculate the transport coefficients in the Langevin dynamics and on the hadronization hypersurface. We have employed the publicly available ideal 2+1-dimensional AZHYDRO code [40] in our study. It assumes longitudinal boost invariance [46] and has been tuned to fit to bulk observables at kinetic freeze-out at an energy density of $e_{\rm fo} = 0.075$ GeV/fm^3 in $\sqrt{s_{NN}} = 200$ GeV Au+Au collisions at RHIC [40]. The initialization of AZHYDRO is done at $\tau_0 = 0.6$ fm/c by specifying the entropy density distribution as

$$s(\tau_0, x, y; b) = \kappa[\frac{1}{4} n_{\rm BC}(x, y; b) + \frac{3}{4} n_{\rm WN}(x, y; b)] \ , \quad (6)$$

where $n_{\rm BC}$ and $n_{\rm WN}$ are the binary-collision and wounded-nucleon densities, respectively, calculated in the optical Glauber model [40], and b is the impact parameter. The coefficient κ is fitted to the observed rapidity density of charged hadrons, $dN_{\rm ch}/dy$, and translates into an initial entropy density of $s(\tau_0, 0, 0; 0) = 110$/fm^3 at the center of the transverse plane for central Au+Au collisions at RHIC.

In Fig. 3 we summarize the main features of AZHYDRO relevant to our HQ diffusion calculations. The upper panel displays the time evolution of the energy-momentum anisotropy, $\epsilon_p = \langle T^{xx} - T^{yy} \rangle / \langle T^{xx} + T^{yy} \rangle$ for semi-central collisions (b=7 fm); it exhibits the development of the bulk anisotropy which leads to an elliptic flow for final-state particles [40]. One sees that ϵ_p tends to saturate at later times when the spatial anisotropy of the system has essentially vanished; the dip around $\tau \simeq 5$ fm/c is due to the vanishing acceleration in the mixed phase, which, in turn, is a result of the equation of state (EoS) with a Maxwell construction between a non-interacting QGP with a bag constant, $B = 0.3642$ GeV/fm^3 at $T > T_c = 165$ MeV, and a hadronic resonance gas at $T < T_c$. Since in our Langevin simulations the HQ test particles freeze out at the end of the mixed phase (at $e_{\rm dec} = 0.445$ GeV/fm^3), we show in the middle and lower panels of Fig. 3 the light-quark p_t-spectrum and v_2 at this point, respectively. The light-quark mass is taken as $m_q = 350$ MeV and we used the standard Cooper-Frye freeze-out procedure [40, 47]. For comparison we also show the results of an empirical fireball parametrization of quark distributions extracted from multi-strange hadron spectra in Ref. [48]. The quark-p_t spectra are noticeably harder than in the hydrodynamic evolution. Since multi-strange particles are believed to kinetically decouple close to T_c, this suggests that the hydrodynamic evolution in the default AZHYDRO does not generate enough flow in the QGP. To investigate the effect of a larger flow on HQ spectra we will also conduct Langevin simulations with a schematic fireball whose final-state flow is given by the empirically

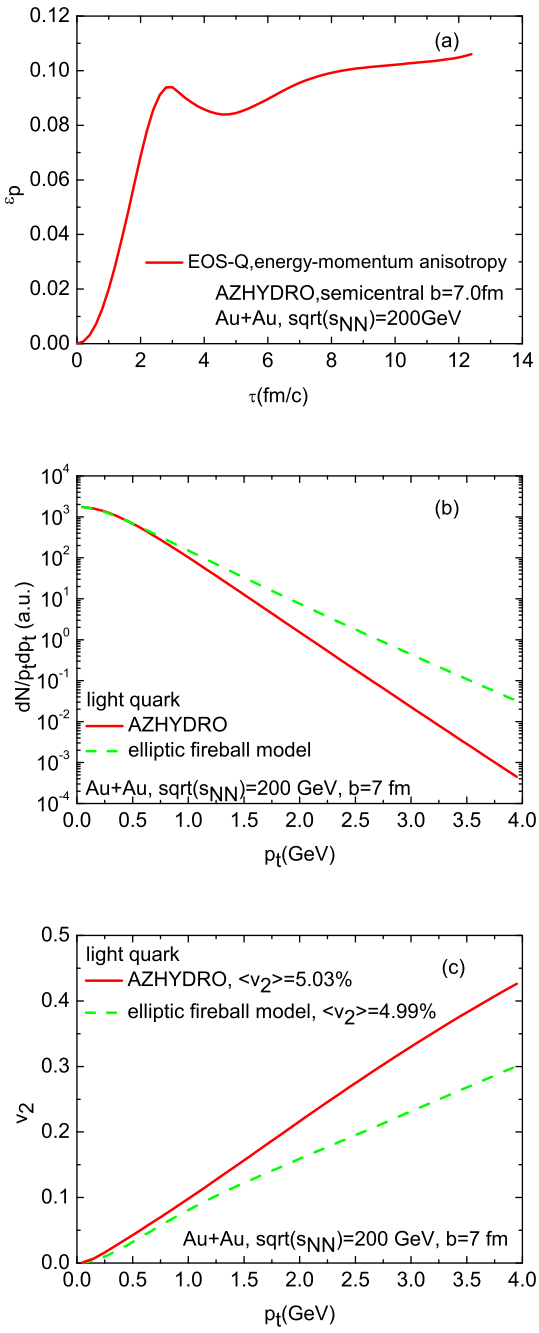

FIG. 3: (Color online) (a) The time evolution of the asymmetry ϵ_p of the energy-momentum tensor in AZHYDRO for $b = 7$ fm Au+Au collisions at $\sqrt{s_{\rm NN}} = 200$ GeV. (b) Light quark ($m_q = 350$ MeV) p_t-spectrum calculated with freeze-out at the end of the mixed phase with decoupling energy density $e_{\rm dec} = 0.445$ GeV/fm^3 in AZHYDRO (red solid line). It is compared to the light quark spectrum at the end of the mixed phase of the parameterized elliptic fireball model discussed in Sec. IV (green dashed line). (c) The light quark elliptic flow v_2 at the end of the mixed phase. Again, AZHYDRO and the parameterized fireball results are shown.

extracted quark spectra. The pertinent elliptic flow exhibits slightly flatter p_t dependence than in the hydrodynamic simulation, cf. lower panel of Fig. 3. However, the integrated quark elliptic flow of $\langle v_2\rangle = 4.99\%$ is very close to the hydro result of $\langle v_2\rangle = 5.03\%$, representing the benchmarks from which the heavy quarks acquire v_2 through heavy-light parton interactions. However, another 20-30% is typically built up in the hadronic evolution below T_c (recall the upper panel of Fig. 3) which is neglected in the present study.

D. Initial Distributions of Heavy Quarks

The number of heavy quarks produced in heavy-ion collisions is consistent with binary nucleon-nucleon collision scaling [49]. Thus their initial spatial distribution is expected to follow the binary collision density, $n_{\rm BC}(x, y; b)$ which we adopt in our simulations within the transverse area where the energy density, $e(\tau_0, x, y)$, is larger than the decoupling value $e_{\rm dec} = 0.445$ GeV/fm^3. For the initial HQ momentum distribution, we use the same spectrum as in Refs. [10, 22], where PYTHIA results for charm- and bottom-quark spectra, converted into D and B mesons via δ-function fragmentation, were tuned to semi-leptonic electron-decay spectra as measured in $p + p$ and d+Au collisions at RHIC. This procedure leads to a bottom-to-charm cross section ratio of $\sigma_{b\bar{b}}/\sigma_{c\bar{c}} = 4.9 \times 10^{-3}$, and a crossing of the electron spectra from D- and B-meson decays at $p_t^e \approx 5$ GeV, see Fig. 4. The b/c cross-section ratio is within the range of pQCD predictions [50] and turns out to reproduce fairly well experimental data [51, 52] for the p_t-dependence of the ratio of electrons from B-mesons to the sum from D+B, cf. lower panel of Fig. 4. The B-meson contribution becomes sizable for $p_t^e \gtrsim 3$ GeV.

E. Heavy-Quark Spectra and Elliptic Flow

We now combine the ingredients as specified in the previous sections to perform the hydro+Langevin simulation of HQ diffusion in the QGP using the test-particle method. A vector $(\mathbf{x}_0, \mathbf{p}_0)$ in transverse phase space, representing a heavy quark, is generated by Monte Carlo methods following the initial distributions discussed in Sec. II D. Then we follow the trajectory of the heavy quark in phase space in equal time steps in the lab frame. At each time step, we read off the temperature, energy density and velocity of the fluid cell at the current HQ position, $(\tau, x, y, \eta = 0)$. The drag coefficient is determined by the HQ momentum in the fluid rest frame and the temperature of the fluid cell. The momentum of the heavy quark is updated stochastically in the fluid rest frame according to the Langevin rule in Eq. (2) and boosted back to the lab frame using the fluid velocity. The HQ position is updated in the lab frame, which can be shown to be equivalent to an update in the fluid rest frame. Test

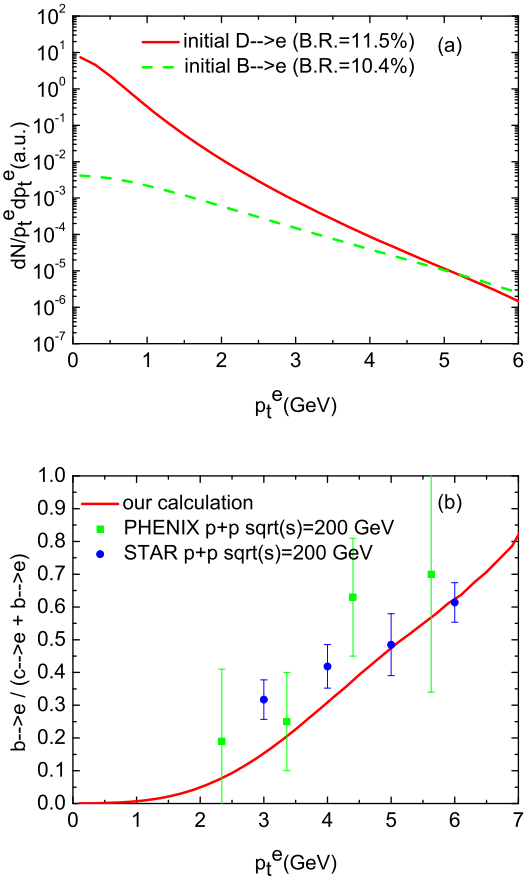

FIG. 4: (Color online) (a) Electron spectra from semileptonic decays of D- and B-mesons (obtained from initial c- and b-quark spectra with δ-function fragmentation) in p+p collisions at RHIC energies. (b) Transverse-momentum dependence of the relative contribution of electrons from B-mesons to electrons from D+B decays. The solid curve results from the spectra in the upper panel which we adopt in our calculations; the data are from PHENIX [51] (filled squares) and from STAR [52] (filled circles) for $p+p$ collisions at $\sqrt{s} = 200\,\mathrm{GeV}$.

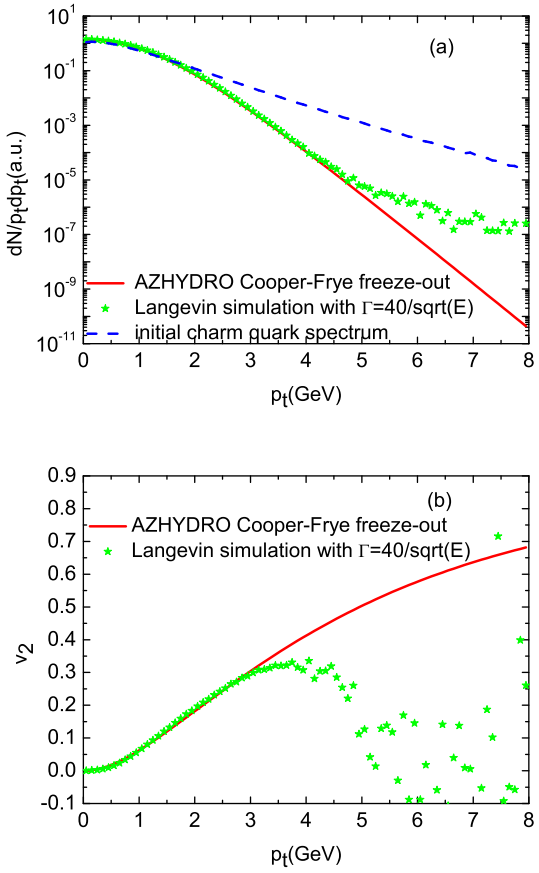

FIG. 5: (Color online) (a) The charm quark p_t-spectrum obtained from hydro+Langevin simulations with a large drag coefficient, $\Gamma = 40.0/\sqrt{E}/\mathrm{fm}$ (dots), compared to the equilibrated charm-quark spectrum calculated from the $e_{\rm dec} = 0.445\ \mathrm{GeV/fm^3}$ freeze-out hypersurface in AZHYDRO (red solid line). The blue dashed line is the initial charm-quark spectrum with the same total yield. (b) The same comparison as in (a) but for the elliptic flow.

particles that have diffused away from $\eta = 0$ to rapidity y and space-time rapidity η are redefined from the longitudinal phase-space coordinate $(\eta; y)$ to $(0; y-\eta)$ to enforce boost-invariance.

The heavy quark continues to diffuse in the QGP until the local energy density of the fluid drops below the decoupling value, $e_{\rm dec} = 0.445\ \mathrm{GeV/fm^3}$, corresponding to the end of the mixed phase of the cell. At that point, we assume the heavy quark to decouple from the fireball and mark it for hadronization. We do not take into account a possible local reheating if the expanding QGP phase "swallows" again an already hadronized heavy quark due to the increasing matter flow. Our criterion for the decoupling of heavy quarks automatically yields their flux across the hadronization hypersurface as

$$f_Q(\tau, x, y; \mathbf{p}) p_\mu d\sigma^\mu(\tau, x, y)/E(\mathbf{p}) \qquad (7)$$

for any area element $d\sigma^\mu(\tau, x, y)$ on that surface, in accordance with the Cooper-Frye formalism for the hydrodynamic freeze-out.

It is critical to verify that heavy quarks can reach local equilibrium as the stationary solution [53]. We have checked the equilibrium limit with an artificially increased drag coefficient, $\Gamma = 40/\sqrt{E\,[\mathrm{GeV}]}/\mathrm{fm}$, and a homogeneous initial spatial distribution for test particles in the transverse plane. This specific choice for the energy dependence of Γ resembles the momentum dependence of the T-matrix based coefficients.[1] The size of the numerical coefficient ($\sim$40) in the large-Γ case is

[1] We have verified that the higher-order terms in Eq. (5), which are dropped in our Langevin simulations below, are negligible for the much smaller "realistic" coefficients.

limited by the requirement that the numerical time-step in the Langevin process be smaller than the inverse relaxation rate. In the upper panel of Fig. 5 the Langevin charm-quark spectrum with large coefficients is compared to the distribution from Cooper-Frye freeze-out on the $e_{\rm dec} = 0.445$ GeV/fm^3 hypersurface in AZHYDRO, i.e., charm quarks in complete local thermal equilibrium. We have adopted a charm-quark mass of $m_c = 1.8$ GeV, corresponding to the in-medium mass at $T_c = 165$ MeV in our simulations [32]. The spectra agree well up to $p_t \simeq 4.0 - 4.5$ GeV. The deviation at higher p_t is due to surface emission of charm quarks with large velocities which escape the active (i.e. $e(\tau, x, y) \geq e_{\rm dec}$) part of the fireball at the earliest times; roughly 1% of heavy quarks at a given high p_t do not suffer collisions, corresponding to the factor ∼100 suppression of spectra from the Langevin simulation relative to the initial distribution at large p_t. A matching picture is observed for the elliptic flow (lower panel in Fig. 5): at low p_t the v_2 of the hydro+large-Γ-Langevin simulation follows the v_2 of equilibrated charm quarks, while it breaks away and oscillates around zero for large p_t (deviations set in slightly earlier than for the inclusive p_t spectra, presumably since v_2 is a more differential and thus more "fragile" quantity).

Next we turn to the results of our simulations under "realistic" conditions, using the transport coefficients and initial distributions outlined above, together with temperature-dependent in-medium HQ masses [32]. As usual, the modifications of the HQ spectra in the medium are quantified by the nuclear modification factor and elliptic flow,

$$R_{AA}(p_t, y) = \frac{\frac{dN_{\rm AA}}{dp_t dy}}{N_{\rm coll}\frac{dN_{\rm pp}}{dp_t dy}} \ , \tag{8}$$

$$v_2(p_t, y) = \frac{\int d\phi \frac{dN_{\rm AA}}{dp_t d\phi dy}\cos(2\phi)}{\int d\phi \frac{dN_{\rm AA}}{dp_t d\phi dy}} \ , \tag{9}$$

respectively, where $N_{\rm coll}$ is the estimated number of binary nucleon-nucleon collisions for the centrality bin under consideration. In Fig. 6 we display the charm- and bottom-quark $R_{\rm AA}$ and v_2 at the end of the mixed phase as obtained from hydro+Langevin simulations in semi-central Au+Au collisions (b=7 fm). The approach toward thermalization induces a depletion of heavy quarks at large p_t (quenching) and an enhancement at low p_t enforced by HQ number conservation. At $p_t \simeq 5$ GeV, the charm-quark quenching reaches down to ∼0.4 while bottom quarks are much less affected, with $R_{\rm AA}(p_t$=5 GeV)≃ 0.8. Note that at the same p_t the Lorentz-γ of bottom quarks is significantly smaller than for charm. Radiative contributions to HQ transport are estimated to become competitive with elastic scattering once the non-perturbative effects are suppressed, i.e., above $p_t \simeq$ 4-5 GeV for charm quarks [12] (recall Fig. 2). When using a drag coefficient from pQCD elastic scattering only (including both quarks and gluons with

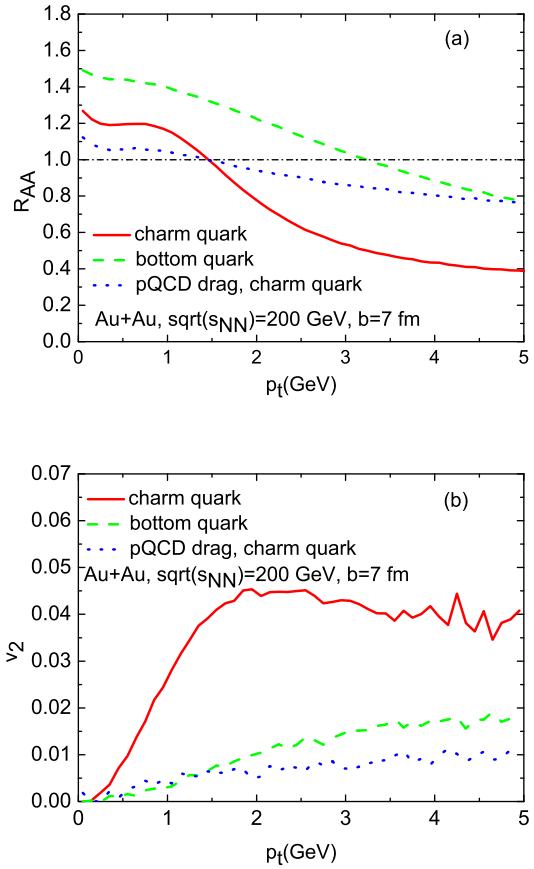

FIG. 6: (Color online) Nuclear modification factor (upper panel) and elliptic flow (lower panel) of charm (red solid line) and bottom quarks (green dashed line) at hadronization obtained from hydro+Langevin simulations for b=7 fm Au+Au collisions at RHIC energy, using transport coefficients from the heavy-light quark T-matrix plus a pQCD HQ-gluon contribution. For comparison charm-quark results are shown with coefficients using only LO pQCD scattering off gluons light quarks (blue dotted line).

$\alpha_s = 0.4$), the quenching is weaker by about a factor of ∼3 [22]. Similar features are found in the elliptic flow coefficient, which for c-quarks first increases approximately linearly before leveling off at about 4.5%, characterizing a transition from a quasi-thermal to a kinetic regime.

Previous calculations employing a thermal-fireball model for the medium evolution, using drag coefficients for non-perturbative elastic scattering [10] of comparable magnitude as in our calculation, have found significantly larger values for the maximal charm-quark v_2 of around 7.5% [22]. Part of this difference originates from the larger "intrinsic" v_2 in the fireball medium which has been adjusted to the empirically observed hadron-v_2 of 5.5-6%. Since the diffusion coefficient of charm (D-mesons) in the hadronic phase is not negligible [54], the HF v_2 in the present study should be considered as a lower bound. Another source of uncertainty derives

from the freeze-out prescription and the associated realization of the HQ Langevin process (Cooper-Frye in the hydro evolution vs. Milekhin-like in some fireball calculations) [55].

III. HEAVY-QUARK HADRONIZATION

The bulk matter in a hydrodynamic simulation can be evolved through a phase transition (here QGP to hadronic matter) solely by specifying the equation of state of the medium. However, the HQ spectra resulting from the Langevin simulations through the QGP are, in general, not in full equilibrium with the bulk medium and thus require a microscopic hadronization mechanism to enable the calculation of HF observables. We will carry this out at the end of the mixed phase, represented by the hypersurface defined by the critical energy density of the hadronic phase in the hydrodynamic simulation. For simplicity we focus on the formation of D- and B-mesons neglecting HF baryons and hidden heavy flavor (both of which have been found to give small contributions to the total HF content of the hadronic phase [22]). Two microscopic hadronization mechanisms have been considered in heavy-ion physics to date: independent fragmentation of partons and coalescence of quarks. The former is appropriate for large-momentum partons emerging directly from initial hard processes, with phenomenological fragmentation functions simulating vacuum gluon radiation and color neutralization. Coalescence, on the other hand, is believed to dominate in the low-momentum regime where partons are abundant in phase-space in heavy-ion [35–37] and even in elementary hadronic reactions [34, 56].

Several previous studies of HQ diffusion in heavy-ion collisions have neglected coalescence processes [25–27, 30], thus limiting the applicability of HF observables to high momenta. The formation time of heavy quarks is comparatively short, and thereafter their virtuality is small, governed by interactions with the medium with modest momentum transfers. Hence, fragmentation is not effective. In the Langevin simulations of Refs. [22–24], heavy-light quark recombination has been accounted for [39] and found to be important for increasing *both* the elliptic flow and the nuclear modification factor of the resulting D-meson spectra. The coalescence formalism was based on the widely used instantaneous approximation [35, 36] which, however, does not conserve energy in the $2 \to 1$ hadron formation process. A related problem is the lack of a well-defined equilibrium limit for the hadron distributions. Together, both features imply appreciable uncertainties in calculating HF observables in the low-p_T region (albeit suppressed compared to light-quark coalescence by a mass ratio (m_q/m_c)). To improve the coalescence description and achieve consistency with local kinetic equilibrium, we here employ the resonance recombination model (RRM) implemented on the hydrodynamic hadronization surface.

A. Resonance Recombination at the Hadronization Hypersurface

In the RRM the hadronization of constituent quarks is treated via resonance scattering within a Boltzmann transport equation [41]. For scattering rates which are large compared to the inverse hadronization time, $\Gamma_{\rm res} \gg 1/\tau_{\rm had}$, equilibrium quark distribution functions in a flowing medium are converted into equilibrium meson spectra with the same flow properties, including elliptic anisotropies with space-momentum correlations characteristic for a hydrodynamically expanding source [48, 57]. The RRM has been employed previously to investigate kinetic-energy and constituent-quark number scaling [57], and to extract empirical quark distribution functions of the bulk medium at hadronization at RHIC [48].

The RRM is consistent with the heavy-light Feshbach resonance formation found in the T-matrix calculation of the HQ thermal relaxation rate (see Section II B). It reiterates the important role played by resonance correlations in our work. As the temperature drops towards T_c, the resonance correlations in the heavy-light quark T-matrix strengthen (recall Fig. 1) and thus naturally merge into heavy-light quark recombination processes. When implementing the latter via a Breit-Wigner ansatz one obtains the HF meson distribution from the asymptotic solution of the Boltzmann equation as [41]

$$f_M^{\rm asymp}(\mathbf{x},\mathbf{p}) = \frac{E_M(\mathbf{p})}{m_M \Gamma_M} \int \frac{d^3p_1 d^3p_2}{(2\pi)^6} f_Q(\mathbf{x},\mathbf{p}_1) \times f_{\bar q}(\mathbf{x},\mathbf{p}_2)\, \sigma(s)\, v_{\rm rel}(\mathbf{p}_1,\mathbf{p}_2)\, \delta^{(3)}(\mathbf{p}-\mathbf{p}_1-\mathbf{p}_2)\ , \quad (10)$$

where $f_{Q,q,M}$ are equal-time phase-space distributions of heavy quarks, light quarks, mesons, respectively, $v_{\rm rel}$ is the relative velocity of the recombining heavy and light quarks, and m_M and Γ_M are the mass and width of the meson resonance [41, 48, 57]. In the calculations below we employ masses and widths compatible with the T-matrix calculation of Ref. [32], extrapolated to $T_c = 165$ MeV with $m_c = 1.8\,$GeV, $m_q = 0.35\,$GeV, $m_D = 2.25$ GeV and $\Gamma_D = 0.1\,$GeV.

Energy conservation and detailed balance in RRM ensure an equilibrium mapping between the distributions of quarks and formed mesons [48, 57]. We verify this in the present case of a non-trivial freeze-out hypersurface given by AZHYDRO. We use local charm- and light-quark equilibrium phase-space distributions, $f(p,x) = e^{-p\cdot u(x)/T}$, with fluid velocities given by AZHYDRO at the end of the mixed phase, then apply resonance recombination, Eq. (10), locally (for each cell) to obtain the local meson phase-space distribution $f_M(\tau,x,y;\mathbf{p})$. Finally we calculate the current across the hypersurface and sum over all fluid cells on the $e_{\rm dec} = 0.445$ GeV/fm^3 freeze-out hypersurface,

$$\frac{dN}{p_T dp_T d\phi dy} = \int_\Sigma \frac{p_\mu d\sigma^\mu(\tau,x,y)}{(2\pi)^3} f_M(\tau,x,y;\mathbf{p})\ . \quad (11)$$

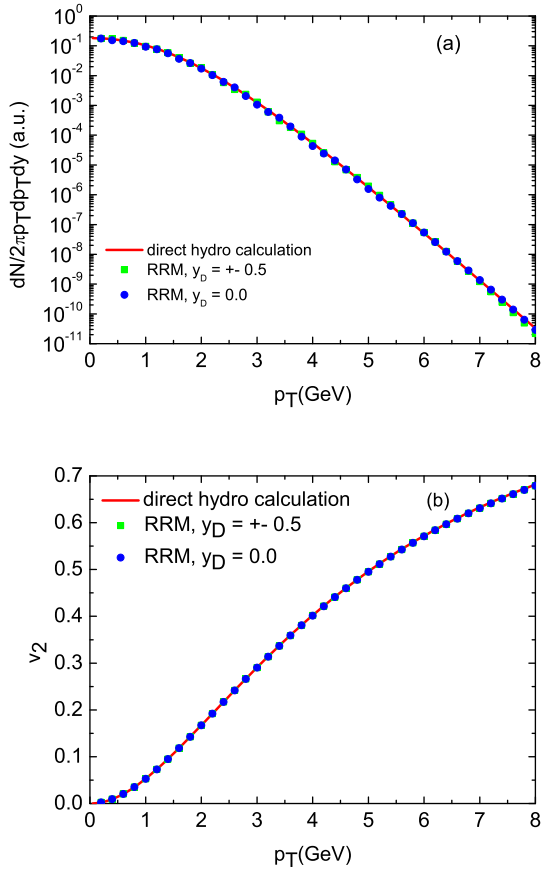

FIG. 7: (Color online) (a) D-meson p_T-spectrum calculated with RRM on the AZHYDRO hadronization hypersurface (circles), compared to a direct calculation from AZHYDRO using the Cooper-Frye formula on the same hypersurface (solid line). The D-meson spectra at different rapidities ($y_D = 0.0$ and $y_D = \pm 0.5$) calculated from RRM agree with each other. (b) The same comparison for the elliptic flow of D mesons.

In Fig. 7 we compare the resulting D-meson spectrum and v_2 with a calculation directly from hydro using D-meson Cooper-Fry freeze-out on the same hypersurface ($e_{\rm dec} = 0.445$ GeV/fm^3). The close agreement of the two calculations verifies the mapping between the equilibrium quark and meson distributions in RRM, including the full space-momentum correlations encoded in the AZHYDRO flow field. Longitudinal boost invariance of AZHYDRO is preserved by RRM as well, as observed from the independence of the D-meson spectra on rapidity within our accuracy.

The next step is to extend our approach to hadronize off-equilibrium quark distribution functions emerging from our HQ Langevin simulations. In order to couple the RRM to a HQ test particle freezing out from the hydro-Langevin simulation with momentum $\mathbf{p}_{\rm dec}$ and coordinate $\mathbf{x}_{\rm dec}$, we represent the corresponding local equal-time HQ phase-space distribution on the hadronization hypersurface, f_Q from Eq. (7), by a δ-function, $\delta^3(\mathbf{x} - \mathbf{x}_{\rm dec})\delta^3(\mathbf{p} - \mathbf{p}_{\rm dec})$ at the hadronization time $\tau(x_{\rm dec}, y_{\rm dec})$. As before, the light-quark phase space density f_q at this point is taken to be the equilibrium distribution $e^{-p\cdot u/T}$ at the local temperature and flow, and we can apply Eq. (10) to obtain the phase space density f_M of heavy mesons test particle by test particle. Finally, the spectrum of heavy mesons follows from Eq. (11) as a sum over test particles. To check our procedure we first apply it to the Langevin output in the large-coefficient limit for charm quarks which – as discussed in Sec. II E – follows the equilibrium distribution up to $p_t \simeq 4$ GeV. Figure 8 shows the comparison between the D-meson spectrum and v_2 calculated in this way and the D-mesons from a direct AZHYDRO calculation. Compared to Fig. 5, the agreement of the hydro+Langevin+RRM calculation with the direct hydro calculation extends to slightly larger p_T since the recombination essentially acts as an additional heavy-light interaction when forming D-mesons. This connection is particularly transparent if the interaction used in the diffusion process is the same as in the recombination process, i.e., a resonance interaction in our approach. We conclude that the equilibrium limit is well under control in this framework.

B. Hadronization: Coalescence vs Fragmentation

After establishing a coalescence formalism for hadronization of off-equilibrium HQ distributions on an arbitrary hypersurface it remains to couple this contribution with the standard fragmentation mechanism representing the large-p_t limit where the phase-space density of light partons vanishes (vacuum limit). In most previous works the coalescence probability has been evaluated in an instantaneous approximation which did not allow for a full control over its absolute magnitude. Here, instead, we use a dynamic criterion which directly follows from the RRM formalism; it is based on the HQ scattering rate which is derived from the same interactions as used in the diffusion calculations[2]. We thus make the following ansatz for the HQ coalescence probability in the fluid rest frame:

$$P_{\rm coal}(p) = \Delta\tau_{\rm res}\ \Gamma_Q^{\rm res}(p)\ , \qquad (12)$$

which is Lorentz invariant. In Eq. (12), the scattering rate, $\Gamma_Q^{\rm res} = n_q \langle \sigma_{qQ}^{\rm res}\ v_{\rm rel}\rangle$, refers to the resonant part of the Qq cross section, $\sigma_{qQ}^{\rm res}$ (or T-matrix), and thus represents the rate for hadron formation (n_q: light-quark density, $v_{\rm rel}$: relative velocity). The time interval $\Delta\tau_{\rm res}$ characterizes the window in the dynamic medium evolution during which resonance states exist; typically, this

[2] See Refs. [23, 54] for a recent discussion of the relation between the two in the HF context

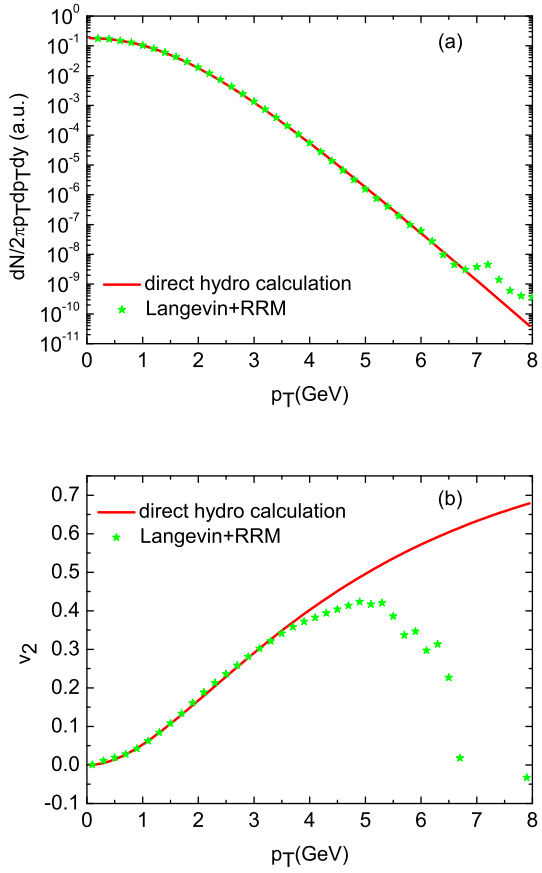

FIG. 8: (Color online) (a) D-meson p_T-spectrum (stars) calculated from RRM on the hadronization hypersurface applied to charm-quark spectra from hydro+Langevin simulations in the large-drag coefficient limit (corresponding to Fig. 5). It is compared to the D-meson spectrum directly calculated from AZHYDRO on the same hypersurface. (b) Same as in panel (a) but for D-meson elliptic flow.

corresponds to the duration of the hadronization transition, i.e., the "mixed phase", or even longer depending on whether "pre-resonance" states can be formed above T_c. Of course, if the product $\Delta\tau_{\rm res}\ \Gamma_Q^{\rm res}$ exceeds one, $P_{\rm coal}$ should be put to one, corresponding to the equilibrium limit (more accurately, one could apply an exponential relaxation, but in view of the practical uncertainties in the values for $\Delta\tau_{\rm res}$ and $\Gamma_Q^{\rm res}(p)$ this is currently not warranted). We emphasize that this procedure provides an absolute normalization of the coalescence contribution, consistent with the (unique) equilibrium limit. Since the resonance formation rate naturally diminishes with increasing HQ momentum (the phase-space density of quarks from the thermal bath to match the resonance mass decreases), one obtains an increasing fraction, $P_{\rm frag}(p) = 1 - P_{\rm coal}(p)$, of heavy quarks undergoing independent fragmentation, recovering the vacuum limit.

In practice, for our calculations reported below, we evaluate Eq. (12) as follows. For the HQ scattering rate we employ a Breit-Wigner cross section which is consistent with our heavy-light T-matrix (cf. Sec. II B) and approximately reproduces the color-singlet contribution to the HQ thermal relaxation rate at T_c; the pertinent meson width of Γ_M=0.4 GeV is larger than the one used in the RRM expression, Eq. (10), but the resulting meson spectra and elliptic flow are rather insensitive to this quantity [41, 57] (we neglect resonant diquark contributions since we only consider color-singlet scattering relevant for D- and B-meson formation). With this cross section we calculate the HQ scattering rate in the fluid rest frame. We typically find $\Gamma_c^{\rm res} \approx 0.1$ GeV for charm quarks at vanishing momentum (similar for bottom quarks), consistent with Refs. [32, 33] (about half of the total HQ width of $\sim$0.2 GeV calculated in these works is due to the color-singlet part).

The HQ scattering rate is then boosted to the lab frame at the end of Langevin simulation (mixed phase) and expressed as a function of HQ transverse momentum. For simplicity, we have chosen to apply $P_{\rm coal}$ not test-particle-by-test-particle but averaged over the spatial dependence in the fireball, i.e., as a function of p_t only. We have checked that the explicit inclusion of space-momentum correlations leads to very similar results for heavy-meson spectra and v_2. For the macroscopic time duration of resonance formation in the medium evolution, we adopt a conservative estimate of $\Delta\tau_{\rm res} \simeq 2\,{\rm fm}/c$ (in the lab frame), amounting to $P_{\rm coal}(p_t \to 0) \to 1$; this is shorter than the duration of the mixed phase in the hydro evolution, $\Delta\tau_{\rm mix} \simeq$ 3-4 fm/c (roughly corresponding to the dip structure in the upper panel of Fig. 3), and thus constitutes a lower limit of the coalescence contribution.

In Fig. 9 we show the coalescence probability, $P_{\rm coal}(p_t)$, for charm and bottom quarks in the lab frame, averaged over all test particles with a given p_t in semi-central (b=7 fm) Au+Au collisions at RHIC. At a given p_t, bottom quarks have smaller velocities than charm quarks and thus more easily find a light-quark partner to recombine with. Consequently, the b-quark coalescence probability drops slower compared to c quarks.

Let us summarize our procedure for HQ hadronization: for each HQ test particle we determine a heavy-meson spectrum for both recombination and fragmentation components, by applying either RRM or a fragmentation function $D_Q(z) = \delta(z-1)$. We then sum over test particles using respective weights $P_{\rm coal}(p_t)$ and $1-P_{\rm coal}(p_t)$, yielding the full coalescence+fragmentation meson spectrum. Thus, the total HF meson spectrum can then be written as

$$\frac{dN_M^{\rm total}}{p_T dp_T d\phi dy} = \frac{dN_M^{\rm coal}}{p_T dp_T d\phi dy} + \frac{dN_M^{\rm frag}}{p_T dp_T d\phi dy}\ . \qquad (13)$$

Note that we determine the absolute normalization of the spectrum by requiring the conservation of HF quantum numbers. Since our fragmentation function automatically conserves HF number we only need to impose the normalization on the recombination contribution to the

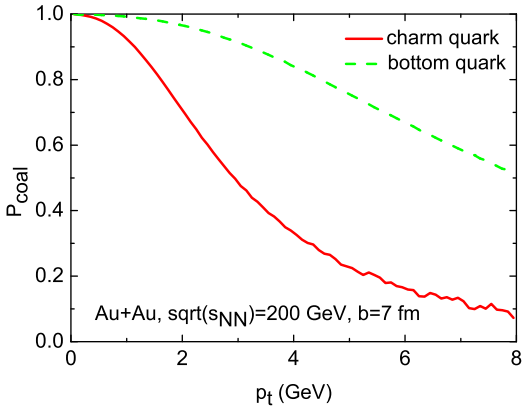

FIG. 9: (Color online) Charm- and bottom-quark coalescence probability as a function of lab-frame p_t for semi-central Au+Au collisions at RHIC.

spectrum. We recall that the formation of heavy quarkonia and heavy baryons has been neglected.

C. Numerical results for D and B mesons

Our final results for the D- and B-meson p_T-spectra and v_2 in semi-central Au+Au collisions at RHIC in the AZHYDRO+Langevin+RRM approach are displayed in Figs. 10 and 11, respectively. The absolute norm of the spectra is arbitrary (we have divided by the number of test particles, 5×10^7, used in our simulations). We also show the individual recombination and fragmentation components in the sum of Eq. (13). The coalescence component dominates over fragmentation up to $p_T \simeq 3(7)$ GeV for D (B) mesons. Below these values, coalescence with light quarks from the hydrodynamic heat bath increases the v_2 by up to 30-40% compared to the HQ v_2 (represented by the fragmentation component), whereas at high p_T the heavy-meson spectra and v_2 approach the fragmentation values.

Rescattering effects due to HQ diffusion in the QGP are also clearly exhibited by the nuclear modification factor which we display in Fig. 12 for D- and B-mesons (as well as for c and b quarks) in semi-central Au+Au collisions at RHIC. We note a dip of the D-meson $R_{\rm AA}$ at low p_T, which is a consequence of the standard mass effect in the collective flow of the D-mesons. Remarkably, the dip is not present in the charm-quark R_{AA}, underlining the effect of the larger D-meson mass and, more importantly, the extra momentum added through coalescence with light quarks. In a sense, coalescence acts as an additional interaction driving the D-meson spectrum closer to equilibrium. The same effect is most likely responsible for the slight suppression of the D-meson spectrum below the c-quark spectrum at high p_T. Again, coalescence acts as an additional interaction towards equilibration,

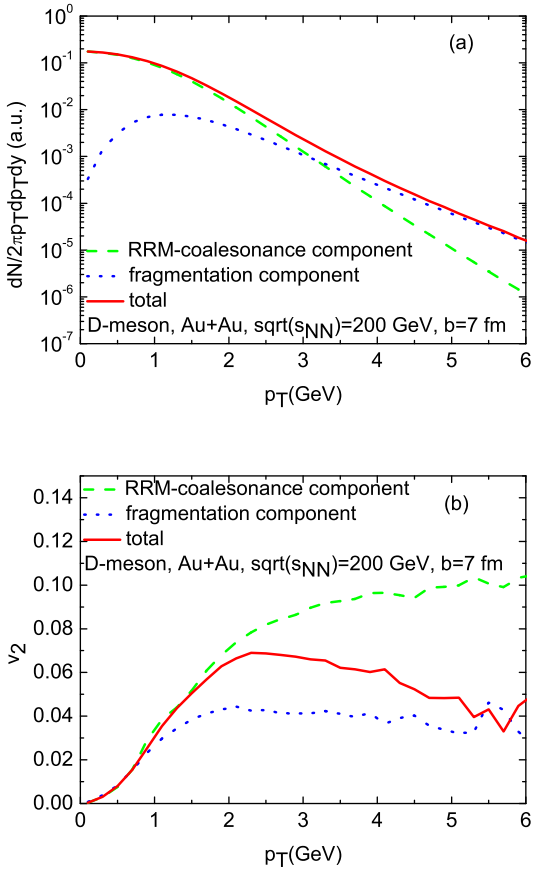

FIG. 10: (Color online) (a) The coalescence, fragmentation, and total D-meson p_T-spectrum for semi-central (b=7 fm) Au+Au collisions at $\sqrt{s_{\rm NN}} = 200$ GeV, normalized to one test particle. (b) The coalescence, fragmentation, and total elliptic flow of D-mesons from the same calculation.

which in this case (high p_T) leads to suppression relative to the c-quark spectrum. This is, in fact, contrary to the naive belief that coalescence should always add momentum to the formed-hadron spectrum. However, the approach toward equilibrium is dictated by the underlying coalescence model (here RRM) possessing the correct equilibrium limit.

The low-p_T D-meson spectrum is rather sensitive to the collective flow in the system. This is not the case for the B-meson spectrum as it does not come close enough to equilibrium, since the thermal b-quark relaxation times are relatively large compared to the system's lifetime. In the following section we quantify how varying the collective flow impacts charm (D-mesons) spectra.

IV. MEDIUM FLOW EFFECT ON D-MESON SPECTRA

In this section, we scrutinize the medium-flow effect on D-meson spectra by comparing our results from

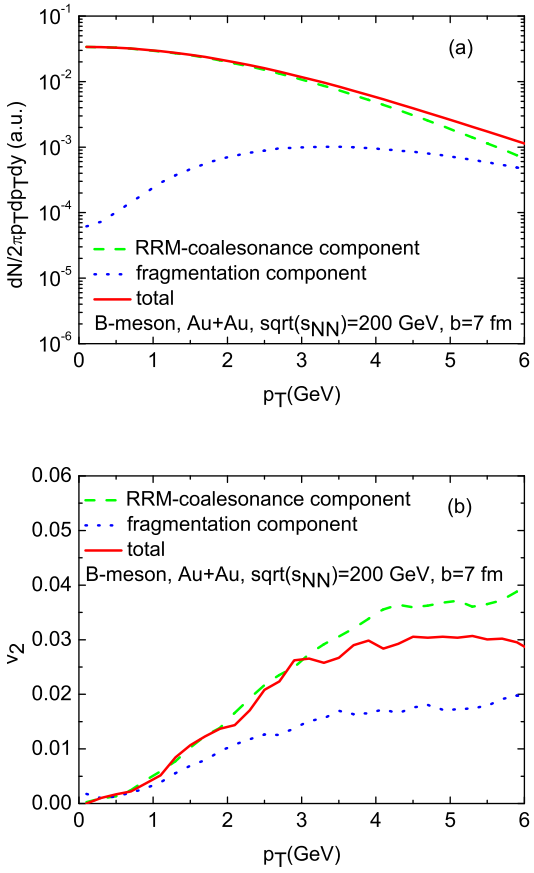

FIG. 11: (Color online) The same as Fig. 10 but for B-mesons.

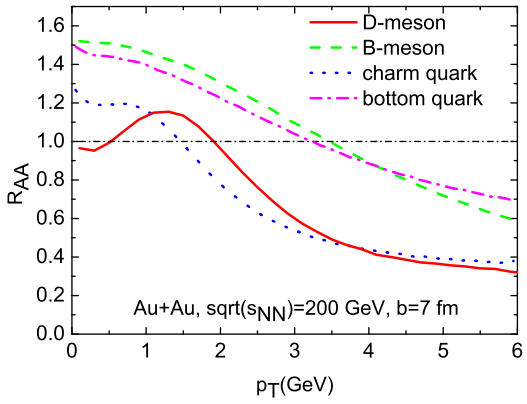

FIG. 12: (Color online) D- and B-meson nuclear modification factors for semi-central (b=7 fm) Au+Au collisions at RHIC. For comparison, the charm and bottom quark $R_{\rm AA}$ are also shown.

the AZHYDRO background with those from a more schematic fireball model. We recall that AZHYDRO employs an EoS with a mixed phase of appreciable time duration over which the sound velocity and thus the acceleration vanish. This is incompatible with state-of-the-art lattice QCD computations [58]. Consequently, AZHYDRO presumably underestimates the flow at the end of the mixed phase and around chemical freeze-out. Rather, it has been tuned to fit bulk observables at kinetic freeze-out, $T_{\rm fo}$=100 MeV, including multi-strange baryons such as the Ω^- [40]. This is in conflict with the general belief (and empirical evidence) that multi-strange hadrons (Ω, Ξ, ϕ) decouple close to T_c (due to their small hadronic rescattering cross sections) but with rather large radial flow [1, 48, 59], thus corroborating our assertion of insufficient flow in AZHYDRO close to T_c.

Instead of retuning AZHYDRO with an improved EoS and/or initial flow [60], we here adopt a modest attitude by investigating flow effects on D-meson spectra with a parameterized elliptic fireball model. We have modified the fireball model introduced in Ref. [22] such that the light-quark p_t-spectrum and its integrated elliptic flow calculated at the end of the medium evolution (QGP + mixed phase) agree with the empirical extraction of Ref. [48] where RRM was applied to experimental multi-strange hadron spectra and v_2. For consistency with the hydro framework we adopt Cooper-Frye freeze-out rather than the Milekhin-like freeze-out in Ref. [22] (cf. Ref. [55]). The retuned fireball results are included in Fig. 3 in direct comparison to those calculated in AZHYDRO. The integrated bulk v_2 extracted from multi-strange particles (4.99%) is close to that calculated in AZHYDRO (5.03%) at T_c, whereas the extracted light-quark spectrum is much harder than in AZHYDRO, due to the larger flow.

We have utilized the fireball evolution to perform charm-quark Langevin simulations with our "realistic" coefficients and to compute D-meson spectra from RRM, summarized in Fig. 13. As expected, the D-meson p_T-spectra, shown in the upper panel for a hadronization with only recombination, are significantly harder compared to using the AZHYDRO background medium. The nuclear modification factor (middle panel of Fig. 13) exhibits a more pronounced flow effect at low momenta. The "flow-bump" for heavy particles is shifted to larger momenta in the fireball compared to AZHYDRO, and the depletion toward $p_T = 0$ is larger. A significant part of this effect originates again from the coalescence process, as can be inferred from comparing the change from the c-quark to D-meson $R_{\rm AA}$ in the "hard" fireball model (middle panel of Fig.13), relative to the "softer" AZHYDRO calculation (Fig. 12), in the intermediate p_T-region. This is, of course, due to the harder light-quark spectrum participating in heavy-light recombination. Also note again that the coalescence D-meson spectrum drops below the c-quark spectrum at high p_T, which once more illustrates the role of resonance recombination as an additional interaction driving the D-meson spectrum toward equilibrium. The total D-meson v_2, shown in the lower panel of Fig.13, receives a modest increase for $p_T \gtrsim 3$ GeV, due to a larger c-quark coalescence probability for stronger

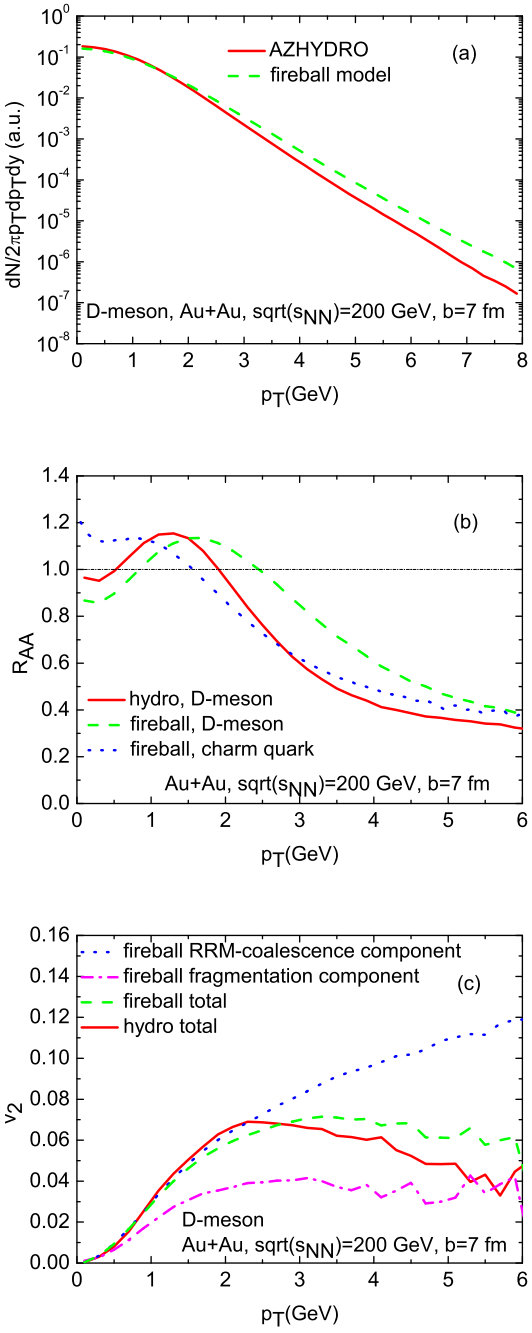

FIG. 13: (Color online) Comparison of D-meson spectra and v_2 from AZHYDRO and an elliptic fireball with larger flow in semi-central (b=7 fm) Au+Au collisions at $\sqrt{s_{\rm NN}}$=200 GeV. (a) p_T-spectra from resonance recombination only (normalized to the same total yield). (b) Nuclear modification factor for D-mesons (coalescence + fragmentation) and charm quarks obtained with the fireball model. (c) Elliptic flow from coalescence, fragmentation and their weighted sum for the fireball, and the total v_2 from AZHYDRO.

flow (comoving light partons have a higher phase-space density at larger momentum when the flow is larger).

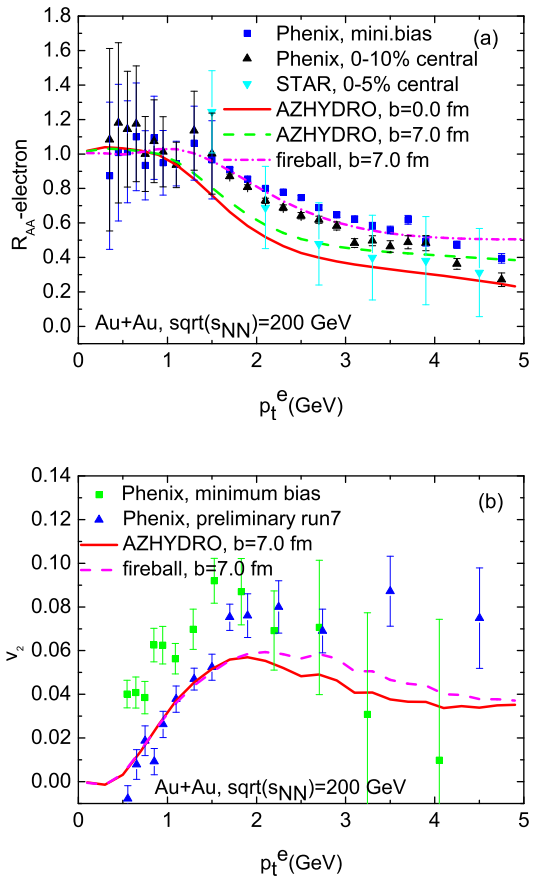

FIG. 14: (Color online) (a) Electron $R_{\rm AA}$ produced from semi-leptonic D- and B-meson decays for central and semi-central Au+Au collisions using hydro and fireball background media, together with data from PHENIX for central and minimum bias collisions [14] and from STAR for central collisions [13]. (b) The same for electron v_2.

V. HEAVY MESON SEMI-LEPTONIC DECAY AND OBSERVABLES

Thus far at RHIC measurements of open HF in Au-Au collisions mostly pertain to their semi-leptonic single-electron decays [13–15].[3] The latter have been shown to preserve the information on the nuclear modification factor and elliptic flow of their parent hadrons rather well [39, 61]. In the following we treat semi-leptonic decays of D- and B-mesons as free quark decays, $c(b) \to s(c) + e + \nu_e$, albeit with effective quark masses equal to their mesonic bound states to correctly account for phase space: m_b=5.28 GeV, m_c=1.87 GeV, m_s=0.5 GeV, m_e=0.0005 GeV and m_ν=0 (light quarks are treated as spectators). We assume an average inclusive electronic

[3] Only very recently have direct D-meson data been reported.

branching ratio of 11.5% and 10.4% for c and b, respectively. We have verified that hadronic form factors have little effect on the electron energy spectrum in the parent-particle rest frame, as already discussed in Ref. [62]. Specifically, the decays are performed via a Monte-Carlo simulation in the HQ rest frame, with the 3-body phase space weighted by the decay matrix element calculated in low-energy $V-A$ theory [62, 63]: $\langle|\mathcal{M}|^2\rangle \propto (p_s{\cdot}p_\nu)(p_c{\cdot}p_e)$ for charm quarks, and $\langle|\mathcal{M}|^2\rangle \propto (p_c\cdot p_e)(p_b\cdot p_\nu)$ for bottom quarks. Subsequently, the electron momentum is boosted to the lab frame using the calculated heavy-meson spectrum.

Our numerical results for the single-electron $R_{\rm AA}(p_t^e)$ and $v_2(p_t^e)$ in Au+Au at RHIC, based on the D- and B-spectra from our hydro+Langevin+RRM (as well as fireball+Langevin+RRM) calculations, are compared to data [13, 14] in Fig. 14. For simplicity, we adopted an impact parameter of b=7(0) fm to mimic the experimental minimum-bias (central) results. On the one hand, the minimum bias sample for bulk observables is closer to b=8-8.5 fm, but, on the other hand, HQ production scales more strongly with centrality, $\sim$A$^{4/3}$, implying a smaller impact parameter for the HF minimum bias sample. Our "conservative" choice of somewhat smaller b could thus slightly overestimate the suppression and underestimate the v_2.

In the upper panel of Fig. 14 one sees that the hydro-based calculations overestimate the suppression found in the experimental data for R_{AA}^e in the regime where the uncertainty of the latter is relatively small. The fireball calculations with larger (and probably more realistic) flow improve on this aspect, which reiterates the importance of medium collectivity in the recombination process. For the elliptic flow (lower panel of Fig. 14) we find good agreement of both calculations with PHENIX run-7 data up to $p_t^e \simeq 1.5$ GeV, whereas the run-4 data are underpredicted. At larger p_t^e our calculations tend to underestimate the run-7 v_2 data. This indicates that additional contributions to charm and bottom interactions are required, e.g., non-perturbative HQ-gluon scattering (presently we treat this part perturbatively), radiative scattering and diffusion of HF hadrons in the hadronic phase [12]. We have recently estimated the charm diffusion coefficient in the dense hadronic phase to be comparable to the values in QGP that we use here [54].

VI. SUMMARY AND CONCLUSION

In this work, we have developed a framework in which heavy-quark diffusion and hadronization in a quark gluon plasma are evaluated consistently in a strongly coupled (non-perturbative) scenario. The strong coupling is realized by resonance correlations which build up in the hadronic channels of anti-/quark correlation functions as the system cools down toward T_c. On the one hand, HQ transport has been based on heavy-light quark T-matrices (consistent with vacuum spectroscopy and the pQCD limit of high-energy scattering), in which meson and diquark resonances enhance the HQ relaxation rate over perturbative calculations [32, 33]; these coefficients have been utilized in relativistic Langevin simulations of HQ diffusion with a medium evolution described by an ideal hydrodynamic model (which itself is based on the strong-coupling limit). On the other hand, as the medium temperature drops towards the critical value, the resonance correlations strengthen and naturally trigger heavy-light quark recombination, which is carried out in the RRM formalism. We have verified the equilibrium mapping between quark- and meson-distributions on non-trivial hadronization hypersurfaces in the hydrodynamic medium, which, in particular, allowed us to identify and quantify the important effect of the medium flow on the D-meson spectrum. We have also given a more rigorous definition of the coalescence probability in terms of the underlying formation rate, and in this way determined the partition between recombination and fragmentation contributions to the heavy-light spectra in absolute terms. We recover the mandatory limits of equilibrium and independent fragmentation for low and large transverse momenta, respectively.

Despite a few missing components in our HQ-transport and hadronization scheme (as discussed below), we have carried our calculations to the level of HF observabels in heavy-ion collisions. In particular, we predict that the degree of charm-quark thermalization is large enough to develop a characteristic "flow-bump" in the D-meson nuclear modification factor. The proper equilibrium limit of the underlying coalescence mechanism is essential in developing this feature, while its location in p_T is sensitive to the strength of the medium flow. For b-quarks the coupling to the medium is not strong enough for this feature to emerge. We have further decayed our D- and B-meson spectra semi-leptonically; the corresponding single-electron spectra show an encouraging agreement with current RHIC data for $p_t^e \leq 2$ GeV; the nuclear modification factor reiterates the importance of a realistic flow strength, while the elliptic flow is a more sensitive gauge for the magnitude of the HQ transport coefficient. Our current estimate confirms earlier results for the spatial diffusion constant in the vicinity of $5/(2\pi T)$.

Several uncertainties and areas of improvement remain, e.g., (i) a more complete evaluation of HQ relaxation rates by including non-perturbative effects in elastic scattering off gluons, as well as adding radiative processes (expected to become relevant at high p_t); (ii) hadronic diffusion, especially in light of recent estimates indicating comparable strength of HF transport in the hadronic and QGP phases near T_c [54]; (iii) a more complete hadro-chemistry at T_c including strange D-mesons and charmed baryons; (iv) a possible Cronin effect in the initial HQ spectra, which mostly affects R_{AA}; (v) further improvements in the medium evolution, i.e., a hydrodynamic background with harder spectra (e.g., due to viscosity, initial flow or a harder EoS). The framework put forth in this paper allows us to systematically address

all of these items. This will not only be beneficial for the open heavy-flavor sector (and an ultimate determination of the QGP's viscosity) but also for its impact on closely related observables such as heavy quarkonia and intermediate-mass dileptons.

Acknowledgments

We gratefully acknowledge helpful discussions with H. van Hees, V. Greco and X. Zhao, and we would like to thank E. Frodermann for his support with AZHYDRO. We are indebted to F. Riek for providing his results for the HQ transport coefficients. This work was supported by the U.S. National Science Foundation (NSF) through CAREER grant PHY-0847538 and grant PHY-0969394, by the A.-v.-Humboldt Foundation, by the RIKEN/BNL Research Center and DOE grant DE-AC02-98CH10886, and by the JET Collaboration and DOE grant DE-FG02-10ER41682.

[1] J. Adams *et al.* [STAR Collaboration], Nucl. Phys. **A757**, 102-183 (2005); K. Adcox *et al.* [PHENIX Collaboration], Nucl. Phys. **A757**, 184-283 (2005); I. Arsene *et al.* [BRAHMS Collaboration], Nucl. Phys. **A757**, 1-27 (2005); B. B. Back, M. D. Baker, M. Ballintijn, D. S. Barton, B. Becker, R. R. Betts, A. A. Bickley, R. Bindel *et al.*, Nucl. Phys. **A757**, 28-101 (2005).
[2] J. Schukraft [for the ALICE Collaboration], *Preprint* arXiv:1103.3474 [hep-ex]; S. Chatrchyan *et al.* [CMS Collaboration], *Preprint* arXiv:1102.1957 [nucl-ex]; G. Aad *et al.* [Atlas Collaboration], Phys. Rev. Lett. **105**, 252303 (2010) [arXiv:1011.6182 [hep-ex]].
[3] M. Gyulassy, L. McLerran, Nucl. Phys. **A750**, 30-63 (2005).
[4] E. Shuryak, Prog. Part. Nucl. Phys. **62**, 48-101 (2009).
[5] S.A. Voloshin, A.M. Poskanzer and R. Snellings, arXiv:0809.2949 [nucl-ex].
[6] D. Teaney, J. Lauret, E. V. Shuryak, [nucl-th/0110037];
[7] U.W. Heinz, arXiv:0901.4355 [nucl-th].
[8] T. Hirano, P. Huovinen and Y. Nara, arXiv:1012.3955 [nucl-th].
[9] B. Svetitsky, Phys. Rev. **D37**, 2484-2491 (1988).
[10] H. van Hees, R. Rapp, Phys. Rev. **C71**, 034907 (2005).
[11] G. D. Moore, D. Teaney, Phys. Rev. **C71**, 064904 (2005).
[12] R. Rapp and H. van Hees, in *Quark-Gluon Plasma 4* (R. Hwa and X.N. Wang, eds.), World Scientific (Singapore, 2010), 111; and LANL eprint arXiv:0903.1096 [hep-ph].
[13] B. I. Abelev *et al.* [STAR Collaboration], Phys. Rev. Lett. **98**, 192301 (2007).
[14] A. Adare *et al.* [PHENIX Collaboration], Phys. Rev. Lett. **98**, 172301 (2007).
[15] A. Adare *et al.* [PHENIX Collaboration], [arXiv:1005.1627 [nucl-ex]].
[16] M. Gyulassy, I. Vitev, X. -N. Wang, B. -W. Zhang, In *Hwa, R.C. (ed.) et al.: Quark gluon plasma* 123-191. [nucl-th/0302077]; A. Majumder, M. Van Leeuwen, [arXiv:1002.2206 [hep-ph]].
[17] S. Wicks, W. Horowitz, M. Djordjevic, M. Gyulassy, Nucl. Phys. **A784**, 426 (2007).
[18] Y.L. Dokshitzer, D.E. Kharzeev, Phys. Lett. **B519**, 199 (2001).
[19] B.-W. Zhang, E. Wang, X.-N. Wang, Phys. Rev. Lett. **93**, 072301 (2004).
[20] E. Braaten and M.H. Thoma, Phys. Rev. **D44**, 2625 (1991).
[21] M.G. Mustafa, Phys. Rev. C **72**, 014905 (2005).
[22] H. van Hees, V. Greco, R. Rapp, Phys. Rev. **C73**, 034913 (2006).
[23] H. van Hees, M. Mannarelli, V. Greco and R. Rapp, Phys. Rev. Lett. **100**, 192301 (2008).
[24] P. B. Gossiaux, J. Aichelin, Phys. Rev. **C78**, 014904 (2008).
[25] Y. Akamatsu, T. Hatsuda, T. Hirano, Phys. Rev. **C79**, 054907 (2009).
[26] S. K. Das, J.-e Alam, P. Mohanty, Phys. Rev. **C80**, 054916 (2009).
[27] W. M. Alberico, A. Beraudo, A. De Pace, A. Molinari, M. Monteno, M. Nardi, F. Prino, [arXiv:1101.6008 [hep-ph]].
[28] B. Zhang, L.-W. Chen, C.-M. Ko, Phys. Rev. **C72**, 024906 (2005).
[29] D. Molnar, Eur. Phys. J. **C49**, 181-186 (2007).
[30] J. Uphoff, O. Fochler, Z. Xu, C. Greiner, Phys. Rev. **C82**, 044906 (2010).
[31] B. L. Combridge, Nucl. Phys. **B151**, 429 (1979).
[32] F. Riek and R. Rapp, Phys. Rev. C **82**, 035201 (2010).
[33] F. Riek and R. Rapp, New J. Phys. **13**, 045007 (2011).
[34] R. Rapp, E. V. Shuryak, Phys. Rev. **D67**, 074036 (2003).
[35] R. J. Fries, B. Muller, C. Nonaka, S. A. Bass, Phys. Rev. Lett. **90**, 202303 (2003); R. J. Fries, B. Muller, C. Nonaka, S. A. Bass, Phys. Rev. **C68**, 044902 (2003).
[36] V. Greco, C. M. Ko and P. Levai, Phys. Rev. C **68**, 034904 (2003).
[37] R.J. Fries, V. Greco and P. Sorensen, Ann. Rev. Nucl. Part. Sci. **58**, 177 (2008).
[38] Z.-w. Lin, D. Molnar, Phys. Rev. **C68**, 044901 (2003).
[39] V. Greco, C. M. Ko, R. Rapp, Phys. Lett. **B595**, 202 (2004).
[40] P. F. Kolb, U. W. Heinz, In *Hwa, R.C. (ed.) et al.: Quark gluon plasma* 634-714, [nucl-th/0305084]; P. F. Kolb, J. Sollfrank, U. W. Heinz, Phys. Rev. **C62**, 054909 (2000).
[41] L. Ravagli, R. Rapp, Phys. Lett. **B655**, 126 (2007).
[42] E. M. Lifshitz and L. P. Pitaevskii, *Physical Kinetics*, Pergamon Press, New York (1981).
[43] J. Dunkel and P. Hänggi, Phys. Reps. **471**, 1 (2009).
[44] M. He *et al.*, *in preparation.*
[45] O. Kaczmarek, F. Zantow, Phys. Rev. **D71**, 114510 (2005); O. Kaczmarek, PoS **CPOD07**, 043 (2007).
[46] J. D. Bjorken, Phys. Rev. **D27**, 140-151 (1983).
[47] F. Cooper, G. Frye, Phys. Rev. **D10**, 186 (1974).

[48] M. He, R. J. Fries, R. Rapp, Phys. Rev. **C82**, 034907 (2010).
[49] S.S. Adler *et al.* [PHENIX Collaboration], Phys. Rev. Lett. **94**, 082301 (2005).
[50] M. Cacciari, P. Nason, R. Vogt, Phys. Rev. Lett. **95**, 122001 (2005).
[51] A. Adare *et al.* [PHENIX Collaboration], Phys. Rev. Lett. **103**, 082002 (2009).
[52] M. M. Aggarwal *et al.* [STAR Collaboration], Phys. Rev. Lett. **105**, 202301 (2010).
[53] D. B. Walton, J. Rafelski, Phys. Rev. Lett. **84**, 31-34 (2000).
[54] M. He, R. J. Fries and R. Rapp, arXiv:1103.6279 [nucl-th].
[55] P. B. Gossiaux, S. Vogel, H. van Hees, J. Aichelin, R. Rapp, M. He, M. Bluhm, [arXiv:1102.1114 [hep-ph]].
[56] R.C. Hwa, C.B. Yang and R.J. Fries, Phys. Rev. C **71**, 024902 (2005).
[57] L. Ravagli, H. van Hees, R. Rapp, Phys. Rev. **C79**, 064902 (2009).
[58] M. Cheng, N. H. Christ, S. Datta, J. van der Heide, C. Jung, F. Karsch, O. Kaczmarek, E. Laermann *et al.*, Phys. Rev. **D77**, 014511 (2008); A. Bazavov, T. Bhattacharya, M. Cheng, N. H. Christ, C. DeTar, S. Ejiri, S. Gottlieb, R. Gupta *et al.*, Phys. Rev. **D80**, 014504 (2009).
[59] B. Mohanty, N. Xu, J. Phys. G **G36**, 064022 (2009).
[60] P. F. Kolb, R. Rapp, Phys. Rev. **C67**, 044903 (2003).
[61] X. Dong, S. Esumi, P. Sorensen, N. Xu, Z. Xu, Phys. Lett. **B597**, 328-332 (2004).
[62] J. D. Richman, P. R. Burchat, Rev. Mod. Phys. **67**, 893-976 (1995).
[63] D. Griffiths, *Introduction to Elementary Particles*, John Wiley and Sons Inc., New York (1987).